A Simplified Impact Damping Model for Honeycomb Sandwich Using Discrete Element Method and Experimental Data

Nazeer Ahmad, R. Ranganath, and Ashitava Ghosal

Abstract Honeycomb sandwich laminates with aluminum and carbon fiber rein-force polymer (CFRP) face—sheets are widely used in spacecraft structures and aerospace industries. The damping behavior of such structures is reported to improve when the granular particles, called damping particles, are inserted in the honeycomb cells. The discrete element method (DEM) has been successfully used and found to give a reasonably accurate estimate of the impact damping. In DEM formulation, Newton's laws of motion are used to obtain the equations of motions of each damping particle considering the contact forces from immediate neighboring particles and other sources, if any. The use of DEM for the real structure where the number of particles is of order 10^8 or more is inefficient and impractical to perform optimization. In this paper, a damping model dissipating equivalent energy is presented for a system consisting of a small honeycomb sandwich coupon filled with damping particles and has resonance frequencies beyond the bandwidth of the model. The coupon is subjected to a range of harmonic excitations (varying frequency and amplitude). The energy dissipated by the damping particles is estimated by DEM. The normal and tangential components of contact forces are modeled using Hertz's nonlinear dissipative and Coulomb's laws of friction, respectively. Then the parameters of the equivalent damper are obtained which dissipates the same energy. The damping model presented incorporates the effect of fill fraction, particle size, and material, as well as the amplitude and frequency of excitation. The comparisons of the DEM model for some of the load cases are done with the experimental data showing reasonably good agreement. The model presented could be readily incorporated in the FEM model like zero-stiffness proof-mass actuator, and the effect of impact damping can be studied without actually solving the DEM governing the motions of the particles.

Keywords Impact damping · Discrete element method · Honeycomb sandwich · Granular damping particles · Passive vibration isolation · Spacecraft structure

N. Ahmad (✉) · R. Ranganath
ISRO Satellite Centre, Old Airport Road, Bangalore 560017, India
e-mail: nazeer@ursc.gov.in

A. Ghosal
Indian Institute of Science, Bangalore 560012, India

1   Introduction

Composite laminates with aluminum/CFRP face sheets and honeycomb core are widely used in aerospace industries owing to its lightweight and excellent mechanical properties. However, in general, a honeycomb sandwich composite possesses very small, less than 2%, inherent structural damping, which results in excessive resonance responses leading to failure of a structure or the mounted subsystems. The damping characteristic of honeycomb is reported to improve when granular particles are inserted in the core [1, 2].

This technique of using granular particles to enhance the damping characteristics of structures is called particle impact damping (PID). The PID is simple, low cost, and effective in extreme environmental conditions. The damping particles dissipate energy in the form of heat and sound after acquiring it from the vibrating structures by momentum exchange. The dissipation is highly coupled and nonlinear depending mainly on parameters: level and frequency of excitation, density of damping particles, fill fraction, mass ratio, and location of filling. The large number of parameters affecting the damping performance of the particles makes it difficult to develop a model, which could capture the complex interactions taking place. The different modeling techniques available in the literature can be found in [6, 8, 11, 12]. One of the methods that is widely used in the particle assemblage simulation is the discrete element method (DEM) [3]. The DEM alone takes into account the particle-to-particle level interaction, enabling to study the dependence of energy dissipation on a large number of parameters. In DEM, equations of motions of damping particles are obtained using Newton's laws assuming that only the particles in immediate neighborhood affect the motion. The contacts of the particle-to-particle and particle-to-cell walls are modeled using the Hertz's theory and Coulomb's law. The energy dissipation is evaluated for each contact occurring during the vibration. As these computations, require to solve the coupled dynamics of the particle and structures, for large structures the number of damping particles runs into millions, and thus the DEM becomes inefficient. Generally, honeycomb sandwich panels that are used in spacecraft are large, and thus the number of damping particles required to effect the damping characteristic is huge. Thus, the use of DEM is computationally very expensive.

Therefore, the energy dissipation by damping particles filled in a small honeycomb coupon of size 100 mm x 100 mm under sinusoidal excitation is estimated experimentally, for some load cases, and using DEM. Furthermore, the dependence of energy dissipation on the various parameters is studied. Finally, the parameters of an equivalent viscous damper are estimated, which could be readily integrated like a proof-mass actuator enabling prediction of structural responses without solving the actual DEM problem.

2 Mathematical Formulation

A small square-shaped coupon of the honeycomb sandwich, shown in Fig. 1, is considered for assessing the dissipation of energy by damping particles. The coupon is 100 x 100 × 25.4 mm dimension. The coupon is very stiff; a normal mode analysis with a free-free boundary condition shows that the first natural frequency is at 6235.2 Hz and the corresponding mode shape is shown in Fig. 2. In this study, we intend to study the damping behavior of the coupon up to 1000 Hz. The coupon is assumed to be rigid, and therefore, cells of the honeycomb do not rotate and undergo deformation. The equations of the cell walls with respect to a local coordinate system, which is at the geometric center of the cell with an axis parallel to the global axis, is shown in Fig. 1. The cell walls are defined by Eqs. (1). The x-axis of the global coordinate system is along the L-direction of the core and the y-axis is along the W-direction of the core.

$$\bar{z} \pm \frac{h}{2} = 0$$

$$\bar{y} \pm \frac{\sqrt{3}}{2} R = 0$$

$$\bar{x} + \frac{\bar{y}}{\sqrt{3}} \pm R = 0$$

$$\bar{x} - \frac{\bar{y}}{\sqrt{3}} \pm R = 0 \tag{1}$$

The damping particles are constrained to move inside the cell as shown in Fig. 3, when the coupon is vibrated. The damping particles in the cells collide and rub with the walls of the cells and face sheets, as well as between themselves. The rubbing and collision result in momentum transfer and energy dissipation. An impact results
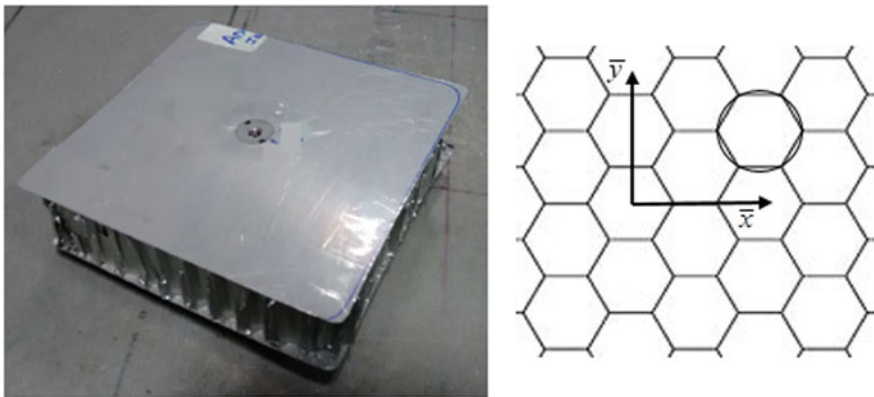

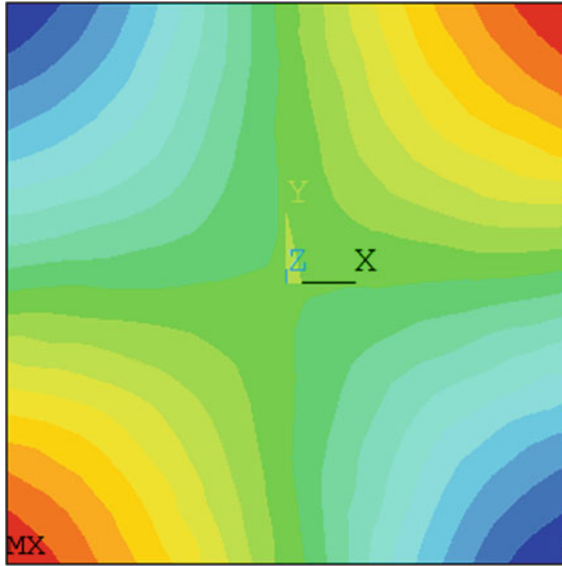**Fig. 1** Honeycomb coupon and axis definition

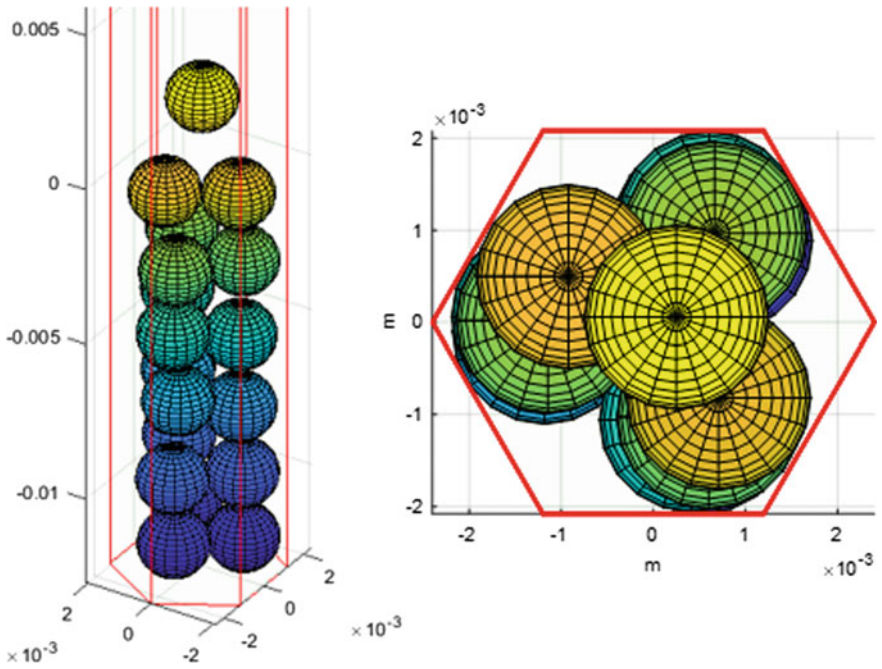**Fig. 2** First mode of the coupon

Fig. 3 Motion of damping particles in a cell

in normal and tangential forces, the normal force is modeled by Hertz's nonlinear dissipative contact model defined in [9], as

$$\mathbf{f}_{ij}^{n} = -\left(k_n\left(\delta_{ij}^{n}\right)^{3/2} + \alpha\sqrt{m_{ij}^{*}k_n}\left(\delta_{ij}^{n}\right)^{1/4}\dot{\delta}_{ij}\right)\mathbf{n}_{ij} \tag{2}$$

where $\dot{\delta}_{ij}^{n}$ is the local indentation velocity and α is the damping constant related to normal restitution coefficient e_n[9], defined as.

$$\alpha = -\ln(e_n)\sqrt{\frac{5}{\ln(e_n)^2 + \pi^2}} \tag{3}$$

The Hertz's constant k_n can be found in [4], and the equivalent mass m_{ij}^{*} in Eq. (2), is defined as

$$m_{ij}^{*} = \frac{m_i m_j}{m_i + m_j} \tag{4}$$

The tangential contact force is modeled the coulomb's law of sliding friction [4], given as

$$\mathbf{f}_{ij}^{t} = -\mu\left|\mathbf{f}_{ij}^{n}\right|\frac{\mathbf{V}_{ij}^{t}}{\left|\mathbf{V}_{ij}^{t}\right|} \tag{5}$$

where μ is the coefficient of friction and $\mathbf{V}_{ij}^{t}$ is the relative tangential velocity of contact points. The change in the velocity and evolution of the forces/moments during an oblique contact process is given in Figs. 4 and 5. Figure 4a–d present the velocity and forces/moments when a damping particle collides with a velocity of [0 0.5–0.1] m/s to the plane, $z = -h/2$. Figure 4c and d show the effect of nonlinear dissipative terms present in the expression for normal force, due to this dissipative term, the relative velocity reaches to zero well before the end of the contact process that can be seen as a small loop at the end of the contact process.

The pre and post-collision velocity and force distributions of the same damping particle colliding again with the plan: $\bar{y} - \sqrt{3}/2R = 0$ is given in Fig. 5a–d. As it is known that the Coulomb's model of friction force, for smaller incidence angles, typically less than 30° [4], does not predict correctly the post collision velocities. However, due to its simplicity and speed, it is extensively used by researcher in vibration problems. One of the consequence of Coulomb's force is the oscillation of tangential force; this phenomenon is clearly visible in time-tangential force plot in Fig. 5d.

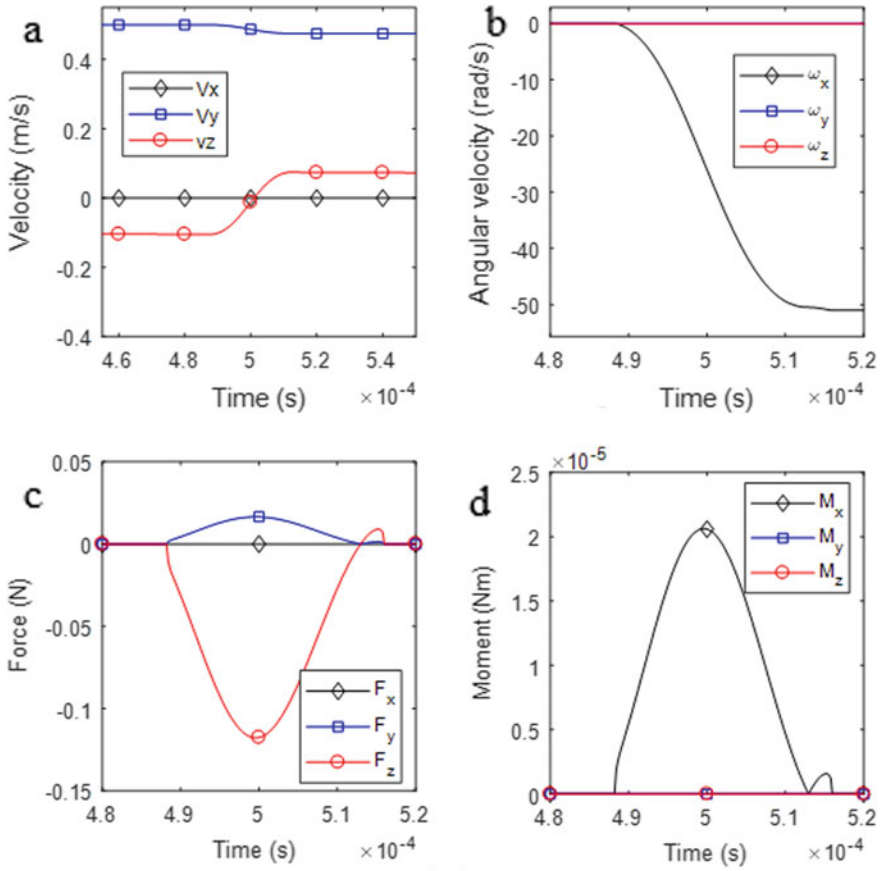The motion of the DPs in the cell can be described by the force and moment balance equations as [2].

Fig. 4 Change in velocities of a particle colliding walls of the cells

$$m_{pi}\ddot{\mathbf{p}}_i = -m_{pi}\mathbf{g} + \sum_{j=1}^{n_1} \mathbf{f}_{ij} + \sum_{w=1}^{n_2} \mathbf{f}_{iw}$$

$$\mathbf{I}_i\ddot{\mathbf{\Phi}}_i = \sum_{j=1}^{n_1}\left(r_i - \frac{\delta_{ij}}{2}\right)\mathbf{n}_{ij} \times \mathbf{f}_{ij} + \sum_{j=1}^{n_2}(r_i - \delta_{iw})\mathbf{n}_{iw} \times \mathbf{f}_{iw} \qquad (6)$$

where the mass of the damping particle is represented by m_{pi}, radius r_i, and moment of inertia $\mathbf{I}_i$. The position vector and angular acceleration of the damping particle is given by $\mathbf{p}_i$ and $\ddot{\mathbf{\Phi}}_i$, respectively. $\mathbf{n}_{ij}$ and $\mathbf{n}_{iw}$ are the unit vectors. $\mathbf{g}$ represents the acceleration due to gravity and the contact forces due to neighboring particle and walls are represented by $\mathbf{f}_{ij}$ and $\mathbf{f}_{iw}$, respectively. The local normal indentations against damping particle and wall are represented by, δ_{ij} and δ_{iw}, respectively.

The DEM formulation requires a very small time step in the integration of equations typically an order less than that of the contact period. In this work, a time step
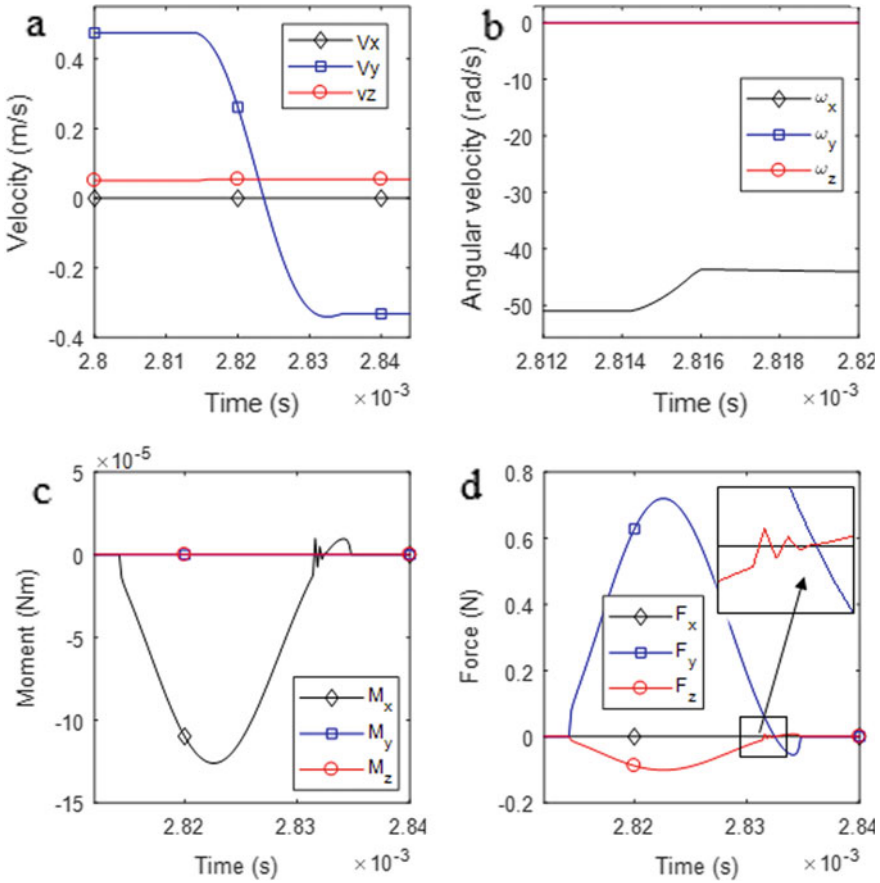
Fig. 5 Change in velocities of a particle colliding walls of the cells (2nd collisions)

of 2×10^{-6} s has been used. The selection of time step is crucial for the success of the DEM, as the new contacts are formed and old contacts are broken leading to change in differential equations being integrated.

The energy dissipated per unit area by the contact forces during the impact as a result of vibration can be written as

$$E_d = \frac{\sum_{k=1}^{N_c} \int_0^{t_c} \left(\alpha \sqrt{m_{ij}^* k_n} \delta^{1/4} \dot{\delta}_{ij} \dot{\delta}_{ij} + f_{ij}^t \dot{\delta}_{ij} dt \right) dt}{A} \tag{7}$$

where t_c is the contact duration, N_c is the number of contacts, A is the area of the coupon and E_d is the energy dissipated. The energy dissipated by Hertz's and Coulomb's forces for a single particle collision described above in two events are given in Fig. 6.
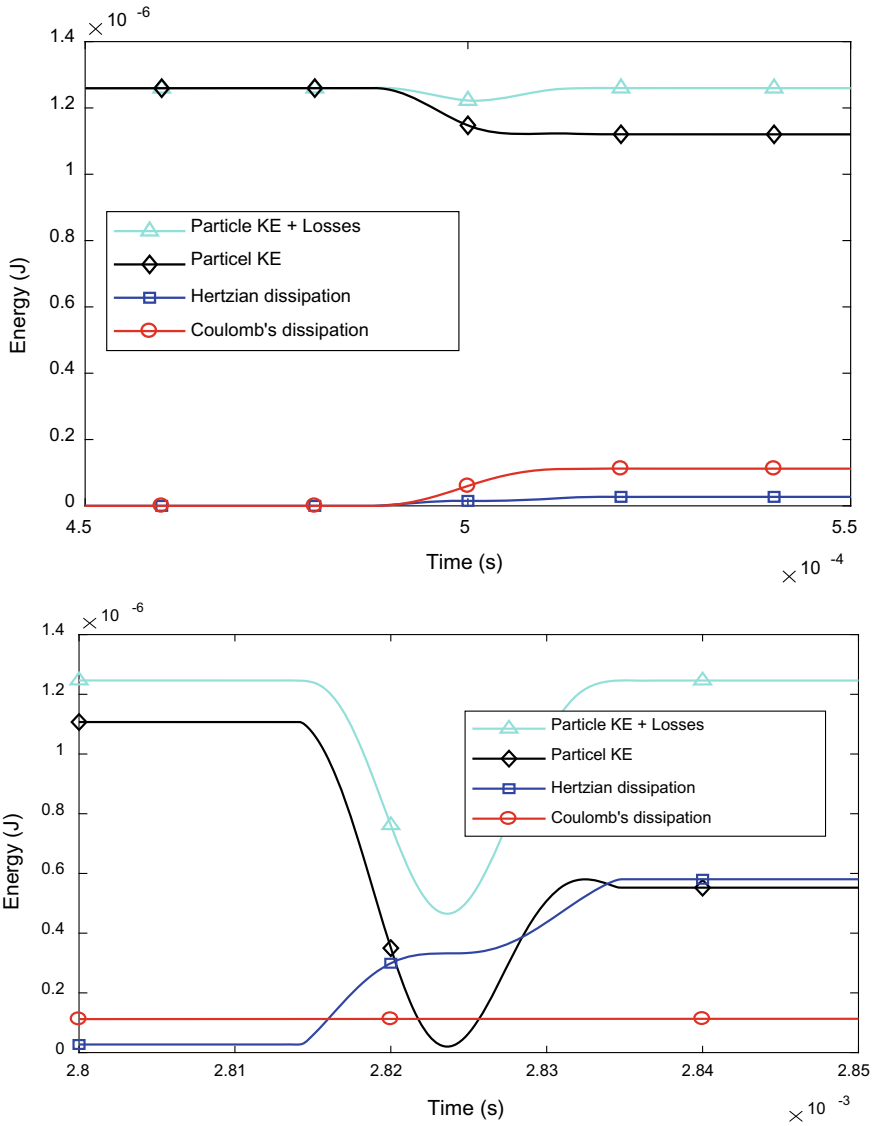
Fig. 6 Energy dissipation prediction by Eq. 7 (1st and 2nd collision)

3 Criterion for PID Performance

The PID dissipates energy by Collison and friction which results in a damping effect on the structure as it takes energy from the structures. As the process is highly nonlinear, the criterion for performance assessment should hold for harmonic, as well as transient vibrations. Specific damping capacity (SDC) is one such parameter

which is used for assessment of the performance of a PID [5]. It is defined as

$$\eta = \frac{\Delta E}{E} \tag{8}$$

where the kinetic energy dissipated per cycle is represented by ΔE, and E is the maximum kinetic energy during the cycle. If the structure is subjected to harmonic excitation of constant acceleration amplitude, then

$$\Delta E = E_d \tag{9}$$

and E is given by

$$E = \frac{1}{2\omega^2} m_c a^2 \tag{10}$$

The specific damping capacity is related to the loss factor as $\eta/2\pi$ and to the linear damping as $-\ln(1-\eta)/4\pi$.

4 Specific Damping Computation and Experimental Validation

The specific damping capacity computation is performed for the acrylic damping particles. The properties of the damping particles are given in Table 1, and the properties of the coupon are given in Table 2. The specific damping capacity is studied with respect to excitation acceleration level, frequency of excitation, and fill fraction as these are the parameters on which SDC is strongly dependent. It is reported in the literature that the density of the DP affects the performance but in the context of the honeycomb structures where it cannot be loaded with metallic particles as it

Table 1 Properties of damping particles

Properties	Units	Aluminum	Acrylic
Radius	mm	1	1.25
Density	kg/m3	2850	1180
Young's modulus	N/m2	70 × 109	2.84 × 109
Poisson's ratio	–	0.33	0.402
Material pairs		Coefficient of sliding friction	Normal restitution coefficient
Aluminum—aluminum	–	0.50	0.85
Acrylic—acrylic	–	0.096	0.70
Acrylic—aluminum	–	0.14	0.70

Table 2 Properties of honeycomb coupon

Properties	Units	Face-sheet (AA 2024 T3)	Honeycomb core (CR 3/16-5056-0.0007-P-32)
Thickness	mm	0.25	25.4
Density	kg/m3	2800	32.1
Young's modulus	N/m2	72×109	$E_{xx} = E_{yy} = E_{zz} = 10000$
Poisson's ratio		0.33	$v_{xy} = v_{yz} = v_{xz} = 0.3$
Shear modulus	N/m2	–	$G_{xy} = 10000$ $G_{yz} = 0.89 \times 10^8$ $G_{xz} = 1.85 \times 10^8$
Diameter of inscribing circle of hexagonal cell	mm	–	4.76

will drastically increase the weight of the structure nullifying the advantage it offers due to its lightweight. Therefore, in this study, light particle like acrylic is used and study with respect to the density of DP is ignored.

5 Experimental Setup

The honeycomb coupon was mounted on a modal shaker (make: M B Dynamics, model: 2050A, Force rating: 100 N) fixed at the center of the coupon. An impedance head (make: PCB, model: 288D01) for measuring the input acceleration and force was fixed between stinger and honeycomb coupon. For measurement of velocity, a PDV-100 Portable Digital Vibrometer was used. The LMS system was used for all data acquisitions. The setup is shown in Fig. 7.

5.1 Computing the Loss Factor Using Experimental Data

The loss factor can be computed from the direct measurement of velocity by laser vibrometer and the input force sensor fixed between the stinger and coupon. Let the f(t) and v(t) represents the instantaneous signals from the force sensor and laser vibrometer, respectively, then the complex power Pc can be expressed as [7, 10]

$$P_c = \frac{1}{T} \int_0^T \left(\sum_{n=0}^{\infty} f_n e^{j(n\omega t - \phi_f)} \right) \left(\sum_m^{\infty} v_m e^{j(m\omega t - \phi_v)} \right) \tag{11}$$

Fig. 7 Experimental setup

The loss factor can be obtained from the complex power Pc as it is the ratio of the real and imaginary parts of the complex power given by Eq. (11). The loss factor can be related to SDC as discussed in Sect. 3. The SDC obtained for some of the load cases is given in Table 3. Three levels of harmonic input acceleration of constant amplitudes of [1 5 10]g at frequency points[50 100 500 1000] Hz for varying fill fractions are computed using the DEM and results are given in Table 3, along with the measured values. The coupon contains 441 cells and each cell can accommodate a maximum of 36 damping particles (100% fill fraction). As the DEM takes 12–16 h of computational time for each load case, and SDC depends on a range of parameters predominantly on fill fraction frequency of excitation and input acceleration amplitude, a multivariate interpolation function is proposed. The interpolating function is obtained using the data given in the Table 3, and the values of SDC at intermediate data points are generated using the interpolation function.

Table 3 Specific damping capacity

Frequency (Hz)	Acceleration (g)	Packing ratio	Specific damping capacity	
			(DEM)	Experimental
50	1	25	1.5702e−4	
		50	0.0018	0.10
		75	0.0051	
		90	0.0089	
	5	25	0.2210	
		50	0.1856	0.23
		75	0.2904	
		90	0.3490	
	10	25	0.1150	
		50	0.2783	0.31
		75	0.3914	
		90	0.4832	
100	1	25	2.9705e−4	
		50	0.0032	0.01
		75	0.0109	
		90	0.0195	
	5	25	0.1836	
		50	0.1891	0.21
		75	0.3158	
		90	0.3190	
	10	25	0.1211	
		50	0.2648	0.32
		75	0.3849	
		90	0.4321	
500	1	25	0.0034	
		50	0.1443	0.22
		75	0.4963	
		90	0.6503	
	5	25	0.1965	
		50	0.5417	0.65
		75	0.8044	
		90	0.8359	
	10	25	0.0975	
		50	0.2770	0.35
		75	0.4145	

Table 3 (continued)

Frequency (Hz)	Acceleration (g)	Packing ratio	Specific damping capacity	
			(DEM)	Experimental
		90	0.4756	
1000	1	25	0.0505	
		50	0.6138	0.71
		75	0.8078	
		90	0.8010	
	5	25	0.1968	
		50	0.5612	0.63
		75	0.8720	
		90	0.8843	
	10	25	0.0911	
		50	0.2886	0.30
		75	0.4444	
		90	0.5305	

6 Variation of SDC with Input Acceleration Amplitudes

Figures 8, 9, 10, 11, 12 show the variation of SDC with respect to input acceleration levels at fill fractions varied from 25%, 50%, 75%, and 90%, respectively. For all the fill fractions SDC increases as acceleration level increased up to 5 g, and thereafter, it is seen decreasing till 10 g. The levels computed using DEM and interpolated are shown in the legend. For low fill fractions, a lower value of SDC can be attributed
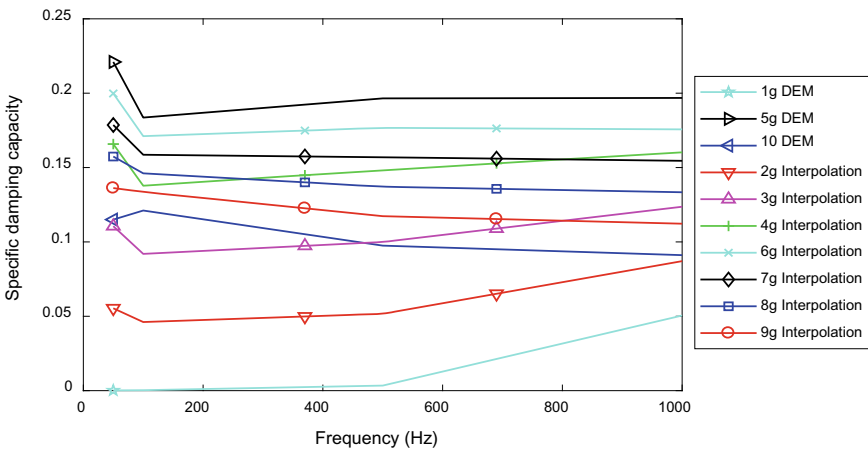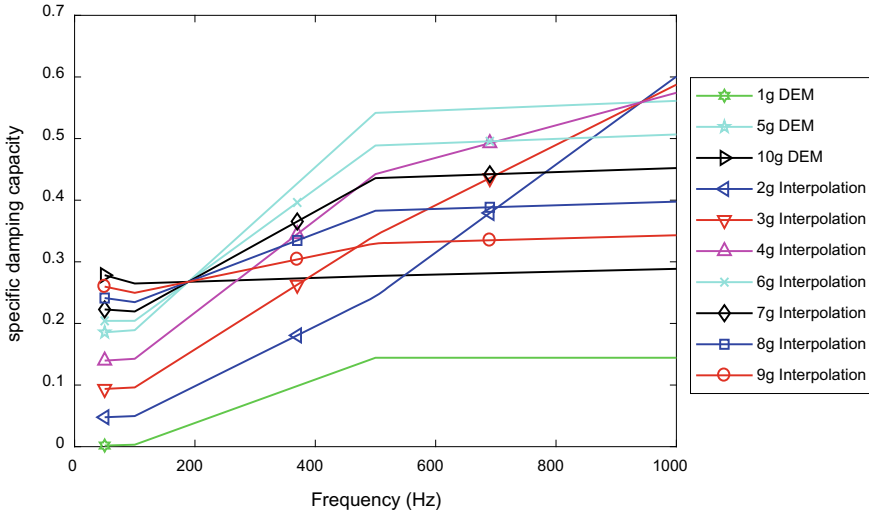

Fig. 8 SDC at 25% fill fraction

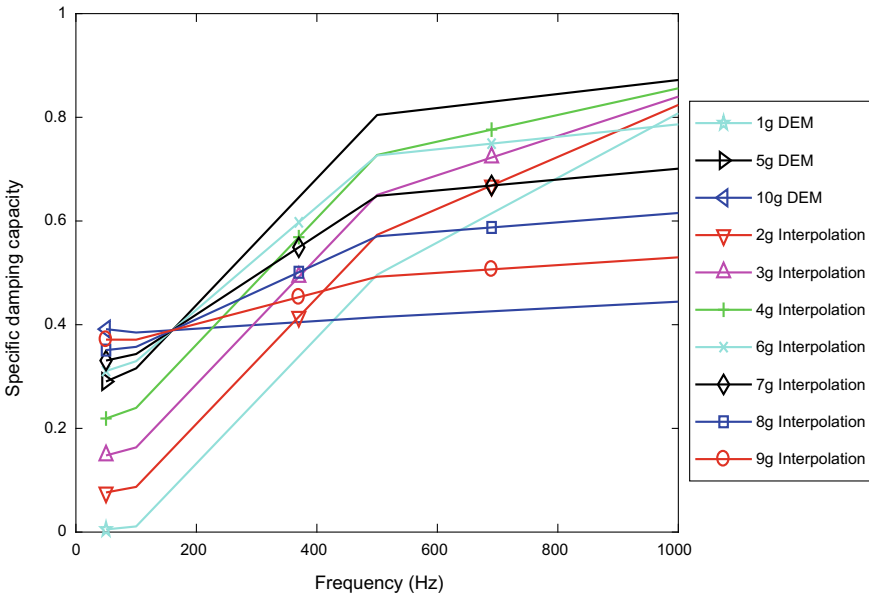**Fig. 9** SDC at 50% fill fraction
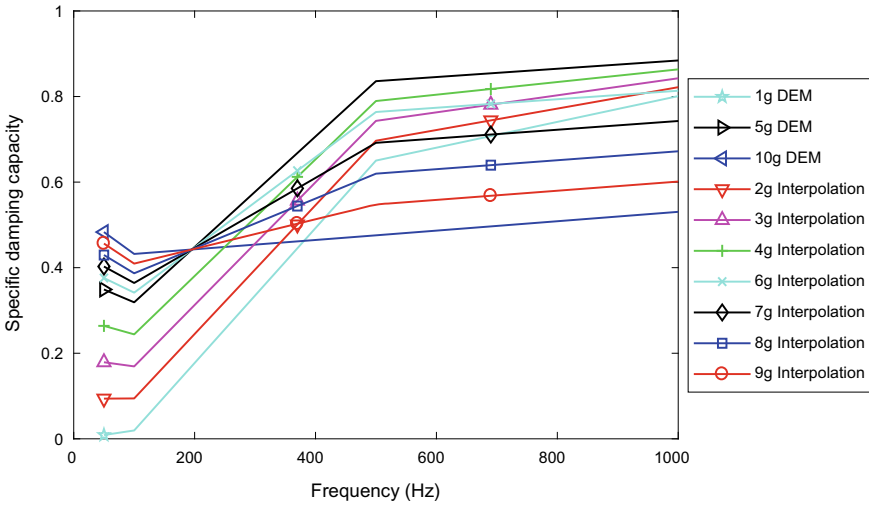

Fig. 10 SDC at 75% fill fraction
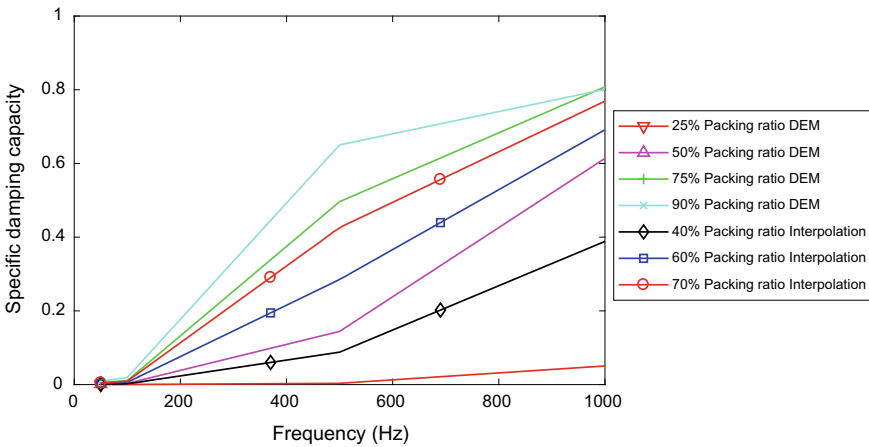
Fig. 11 SDC at 90% fill fraction

Fig. 12 SDC at 1 g acceleration level

to a lesser number of particles in the cell, and thus less number of collisions, and therefore, smaller values of SDC. The value of SDC appears almost constant in the frequency range of study. However, for the fill fractions 50–90%, SDC increased up to 500 Hz and thereafter remains nearly constant.

7 Variation of SDC with Varying Fill Fraction

Figures 12, 13, 14 present the variation of SDC with respect to frequency when the amplitude of harmonic input acceleration is kept constant and the packing ratio is varied. The SDC is seen increasing with respect to frequency at lower acceleration levels for all fill fractions. However, the rate of increase with respect to acceleration level decreases as the acceleration increase. At an acceleration level of 10 g, SDC appears to be independent of frequency. The likely reason for such behavior could be the fact that particles remain most of the time in the cavity space and colliding less frequently with the structure.
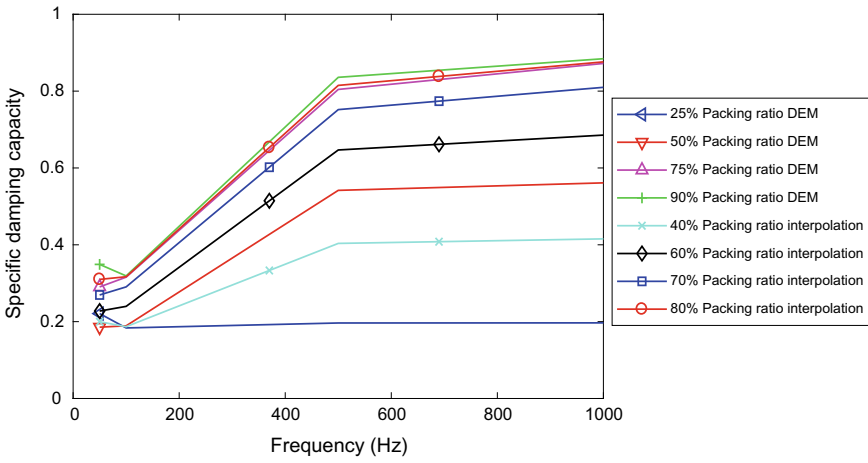

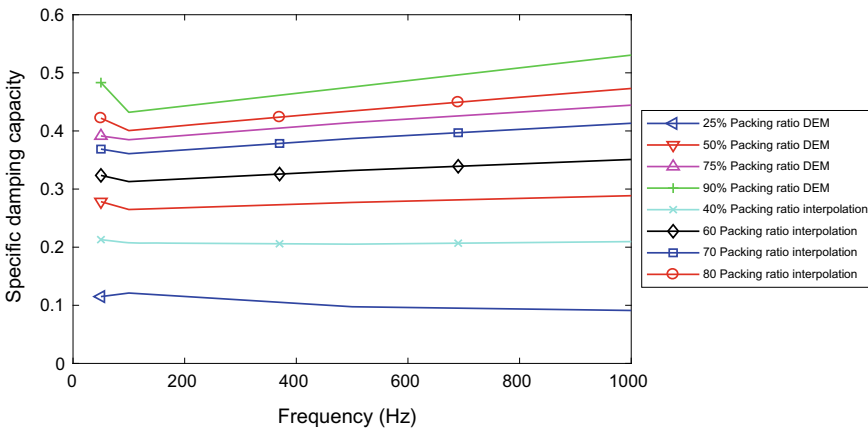**Fig. 13** SDC at 5 g acceleration level

Fig. 14 SDC at 10 g acceleration level

8 Conclusions

The dissipation of energy by the damping particles filled in a small coupon of honeycomb is studied with discrete element method and experimentally. The coupon is vibrated with different levels of constant amplitude harmonic acceleration in a frequency band of 50–1000 Hz with varying amounts of damping particles in the cavity. The energy dissipation is estimated in terms of specific damping capacity and it is found to be dependent on predominantly three parameters: fill fraction, amplitude, and frequency of the input acceleration. A multivariate interpolation model of SDC is worked out using "pchip" interpolant. Using the interpolation, SDC is predicted and presented for various combinations of the variables. The interpolation function developed herewith for SDC can be used for the prediction of the structural response of any honeycomb structure treated with damping particles under harmonic, transient excitation loads.

References

1. Ahmad N, Ranganath R, Ghosal A (2016) Assessment of particle damping device for large laminated structures under acoustic excitations. Presented at the proceedings of 14th ISAMPE national conference on composites (INCCOM-14), Hyderabad
2. Ahmad N, Ranganath R, Ghosal A (2017) Modeling and experimental study of a honeycomb beam filled with damping particles. J Sound Vib 391: 20–34. 2017/03/17
3. Cundall PA, Strack ODL (1979) A discrete numerical model for granular assemblies. Géotechnique 29:47–65
4. Johnson KL (1985) Contact Mechanics. Cambridge University Press
5. Mao K, Wang MY, Xu Z, Chen T (2004) Simulation and characterization of particle damping in transient vibrations. J Vib Acoust 126:202
6. Olson SE (2003) An analytical particle damping model. J Sound Vib 264:1155–1166
7. Romdhane MB, Bouhaddi N, Trigui M, Foltête E, Haddar M. (2013) The loss factor experimental characterisation of the non-obstructive particles damping approach. Mech Syst Signal Process 38: 585–600
8. Saeki M (2005) Analytical study of multi-particle damping. J Sound Vib 281:1133–1144
9. Tsuji Y, Tanaka T, Ishida T (1992) Lagrangian numerical simulation of plug flow of cohesionless particles in a horizontal pipe. Powder Technol 71:239–250
10. Wong CX, Daniel M, Rongong J (2009) Energy dissipation prediction of particle dampers. J Sound Vib 319:91–118
11. Wu CJ, Liao WH, Wang MY (2004) Modeling of granular particle damping using multiphase flow theory of gas-particle. J Vib Acoust 126:196
12. Zhang C, Chen T, Wang X, Li Y (2014) Discrete element method model and damping performance of bean bag dampers. J Sound Vib 333:6024–6037